Applied Clay Science 251 (2024) 107327

Contents lists available at ScienceDirect

Applied Clay Science

journal homepage: www.elsevier.com/locate/clay

Research Paper

Reactive transport modeling of diffusive mobility and retention of TcO_4^- in Opalinus Clay

Ping Chen [a,d,*], Luc R. Van Loon [b], Steffen Koch [c], Peter Alt-Epping [a], Tobias Reich [c], Sergey V. Churakov [a,b]

[a] Institute for Geological Sciences, University of Bern, Bern CH-3012, Switzerland
[b] Laboratory for Waste Management, Paul Scherrer Institut, Villigen PSI CH-5232, Switzerland
[c] Department of Chemistry, Johannes Gutenberg-Universität Mainz, Mainz DE-55099, Germany
[d] Insititute of NuclearApplied Technology, East China University of Technology, Nanchang 330013, Jiangxi, China

ARTICLE INFO

Keywords:
Reactive transport model
Tc
Opalinus Clay
Diffusion
Redox reaction
PFLOTRAN

ABSTRACT

Tc-99 has drawn widespread concern because of its long half-life, high fission yield and high mobility in research of radioactive waste disposal and environmental remediation. TcO_4^- through-diffusion experiments in Opalinus Clay (OPA) were performed under air and under argon No noticeable Tc-breakthrough was observed for over one year while the total Tc concentration in the source reservoir was steadily decreasing under both air and argon atmosphere. The total Tc activity distribution in the clay sample along the diffusion direction was obtained by slicing the OPA clay samples retrieved from the diffusion cells, using the abrasive peeling technique. In the case of diffusion under air atmosphere, almost no Tc was measured in that part of the sample close to source reservoir, while much more Tc was measured under argon atmosphere. A reasonable explanation for this observation is that the reductive retention of Tc plays a significant role during transport. A reactive transport model was constructed to simulate the diffusion process whereby the diffusion of Tc was coupled with redox reactions. Even though reduction of TcO_4^- by aqueous Fe^{2+} is thermodynamically feasible, it was not observed in the experiment. Furthermore, Fe^{2+} associated with solid phase was demonstrated to be more active than aqueous Fe^{2+}. Therefore, surface complexation redox reaction was proposed. Dissolution rate of pyrite, equilibrium constant and diffusion coefficient of TcO_4^- were considered as possible factors controlling the redox reaction. Modeling results showed that TcO_4^- diffused into the clay and was partially reduced into surface complexed Tc(IV) by pyrite. When TcO_4^- transported under air atmosphere, O_2 competitively consumed Fe^{2+} and pyrite, resulting in no Tc immobilization in the related zone.

1. Introduction

Because of high mobility in the environment, long half-life ($T_{1/2}$ = 2.1×10^5 years) and high fission yield in nuclear reactors (Lieser, 2008), ^{99}Tc is one of the important radionuclides in the field of safety assessment of a repository for radioactive waste and for the remediation of subsurface contamination at reprocessing sites (Burgeson et al., 2005; Chatterjee et al., 2020). These properties have stimulated numerous studies on ^{99}Tc geochemical and transport behavior. Tc is a redox sensitive element. Its most stable form in an oxidizing environment is pertechnetate, Tc(*VII*)O_4^-, which is highly soluble (Poineau et al., 2009; Shi et al., 2012; Tagami, 2003). While exposed to reducing conditions, Tc (VII) was reduced to Tc(IV) and precipitates as TcO_2 (Fredrickson et al., 2009; Morris et al., 2008; Peretyazhko et al., 2008), TcS_2-like solids (Lukens et al., 2005; Wharton et al., 2000) and/or was incorporated into iron oxides or sulfides (Peretyazhko et al., 2008; Plymale et al., 2011; Zachara et al., 2007). Thus, reducing conditions significantly limit ^{99}Tc mobility. Consequently, great interest was evoked to the influence of reducing sources in the subsurface, especially in the role of Fe(II) (Huang et al., 2021). Clay minerals play an important role - as host rock and/or as backfill materials - in many repository concepts (ANDRA, 2001; Aoki, 2002; Nagra, 2002; Bonin, 1998; Grambow, 2016; ONDRAF/NIRAS, 2001), and molecular diffusion was identified as the principal mechanism of nuclide transport in such dense clay materials. Numerous diffusion experiments with radionuclides were carried out in clay (Glaus et al., 2015; Joseph et al., 2017; Joseph et al., 2013; Kasar et al., 2016;

* Corresponding author at: Institute for Geological Sciences, University of Bern, Bern CH-3012, Switzerland.
E-mail address: ping.chen@unibe.ch (P. Chen).

https://doi.org/10.1016/j.clay.2024.107327
Received 2 August 2023; Received in revised form 29 February 2024; Accepted 1 March 2024
Available online 7 March 2024

Table 1
Average mineral composition of OPA clay

Mineral	Amount (wt)%
calcite	13 ± 8
quartz	14 ± 4
albite	1 ± 1
potassium feldspar (K-spar)	1 ± 1.6
siderite	3 ± 1.8
pyrite	1.1 ± 0.5
organic carbon	0.8 ± 0.5
illite	23 ± 2
illite/smectite-alternating layer	11 ± 2
chlorite	10 ± 2
kaolinite	22 ± 2

Tachi and Yotsuji, 2014; Van Loon et al., 2003; Wang et al., 2017), including ^{99}Tc (Bruggeman et al., 2010; Li et al., 2012; Tsai et al., 2017; Wu et al., 2014). Though most of these studies improved our knowledge on the Tc behavior in clays in a qualitative way, a quantitative description of the reaction and transport processes is largely missing. Ochs et al. (2001) developed an integrated sorption-diffusion model based on the electric double layer (EDL) theory to predict the apparent diffusivity of TcO_4^- and other nuclides (Ochs et al., 2001; Tachi et al., 2014a; Tachi et al., 2014b) in clays. The drawback of this model is that sorption was characterized with a distribution coefficient (K_d) but no detailed information on the reaction mechanism is included.

In this study, the reactive transport code PFLOTRAN (www.pflotran.org) is used to develop a model that simulates diffusion of ^{99}Tc coupled to chemical (redox) reactions. Important parameters, such as rate constants for mineral reactions and the effective diffusion coefficient for Tc, are calibrated against experimental results. Constraining these parameters based on experimental data is indispensable for predicting the long-term behavior of Tc in the subsurface. Hence, the quantitative model presented here is of great importance for the safety assessment of geological repositories for radioactive waste.

2. Materials and methods

2.1. Opalinus clay

The Opalinus Clay (OPA) used in this study was taken from the Mont Terri (MT) Underground Research Laboratory (URL) in Switzerland (internal charge designation; BLT14). The mineral composition was not determined for this specific sample but an average composition is given in Table 1.

2.2. Diffusion experiments with HTO and $^{99}TcO_4^-$

The design of the through-diffusion experiments on which this study is based, is described in detail in Van Loon et al. (2003). A schematic presentation is shown in Fig. 1. The intact OPA clay sample is sandwiched between two porous steel filters and mounted in a diffusion cell, which is connected with two reservoirs via tubes. Both reservoirs were filled with an artificial OPA pore water.

The composition of the pore water is given in Table 2. The OPA pore water was synthesized following the method described in Pearson (1998).

The pH and alkalinity of the pore water corresponds to the one in equilibrium with the atmospheric pCO_2. In one of the reservoirs, a $^{99}TcO_4^-$ tracer was added to the pore water. This reservoir is further denoted as the source reservoir, while only OPA pore water was placed in the other reservoir which is further denoted as the downstream reservoir. Solutions in both reservoirs were circulated in closed circuits by a peristaltic pump. The experiment under argon atmosphere was performed in a glove box filled with argon at 25 °C, whereas the experiment under air atmosphere was performed in a heating chamber at 60 °C. The pH in the reservoir was 7.6 and 8.4 for diffusion under air and argon atmosphere, respectively. The slightly higher pH of the pore water under argon atmosphere was caused by degassing of the water used for artificial pore water creation, and in the glove box the pCO_2 is close to zero.

Before starting the diffusion experiments, the samples were pre-

Table 2
. Composition of the artificial OPA pore water used in the diffusion experiments.

Ion	Concentration (M)
Na^+	2.40×10^{-1}
K^+	1.61×10^{-3}
Mg^{2+}	1.69×10^{-2}
Ca^{2+}	2.58×10^{-2}
Sr^{2+}	0.505×10^{-3}
Cl^-	3.00×10^{-1}
SO_4^{2-}	1.41×10^{-2}
Alkalinity	0.476×10^{-3}
I (M)	3.90×10^{-1}
pH	7.6

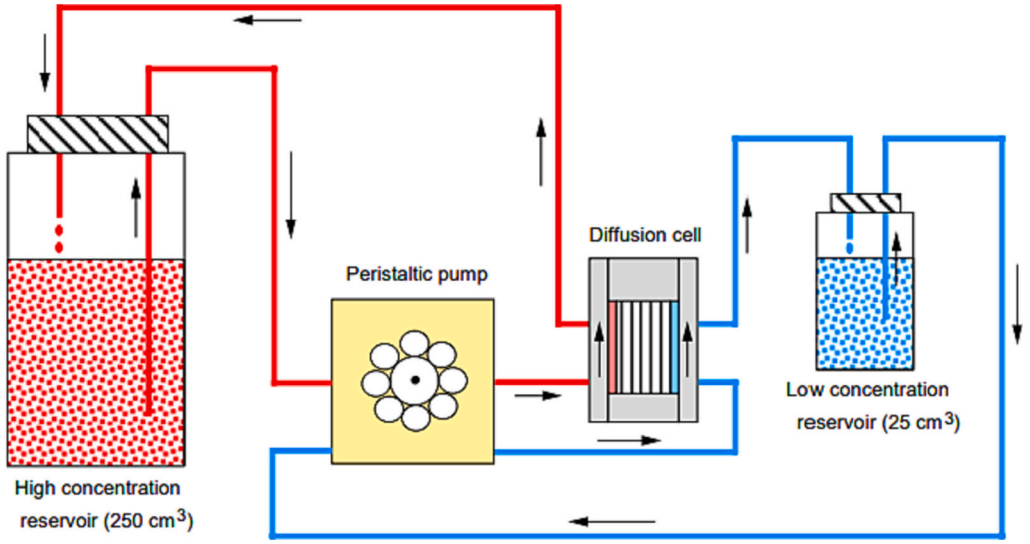

Fig. 1. Scheme of the through-diffusion experimental setup (Van Loon et al., 2003).

conditioned for 4–5 weeks by circulation of the OPA pore water on each side of the samples in order to allow full saturation and chemical equilibrium. After 5 weeks, diffusion of tritiated water (HTO) was initiated, with the diffusion direction being perpendicular to the bedding orientation in both cases. Diffusion of HTO prior to ^{99}Tc was conducted 1) to yield the diffusion parameters (effective diffusion coefficient, D_e, and porosity, φ) of HTO for the clay samples and 2) to check the proper set-up of the diffusion experiment. The source reservoir (210 ml) was spiked with a HTO tracer (approx. 1500 Bq/dm^3). The evolution of HTO in the downstream reservoir (20 ml) was monitored over time by changing the reservoir at regular time intervals and measuring the accumulated activity with Liquid Scintillation Counting (LSC) using a Hidex 300 SL liquid szintillation counter (Hidex) and Ultima Gold™ XR (Perkin Elmer) as scintillation cocktail. When the system reached steady state (constant flux), out-diffusion of HTO was initiated by replacing the solution in both reservoirs with artificial OPA porewater without HTO and repeating the reservoir change process on each side until no more HTO activity could be detected. When HTO had diffused out, the ^{99}Tc tracer (approx. 500 Bq/dm^3) was added to the source reservoir. The evolution of the ^{99}Tc activity in both source and downstream reservoirs was monitored. Small volumes of solutions were sampled and activities were measured by Liquid Scintillation Counting (LSC), using Ultima Gold™ LLT (Perkin Elmer) as scintillation cocktail. It is worth noting that no Tc breakthrough was detected for over one year while the total Tc concentration in the source reservoir was steadily decreasing under both air and argon atmosphere. After about one year, the diffusion experiment with $^{99}TcO_4^-$ was stopped and the OPA clay samples were retrieved from the diffusion cells, air dried and sliced using the abrasive peeling technique described in Van Loon and Eikenberg (2005). This process worked well using a waterproof silicon-carbide P220 sandpaper (type: CP918A; company: VSM). Mass determination for each slice was done by comparing the weight of the individual sample cups (fully prepared with sandpaper) before and after slicing using a precision scale. The theoretical thickness of the individual slices $l_{i,\mathrm{theo}}$ was calculated from the slice weight and sample density, using the following formula:

$$l_{i,theo} = \frac{m_i}{\rho \cdot \pi \cdot \left(r_s^2 - r_c^2\right)}$$

with m_i being the slice mass, ρ the sample density (taken from data sheet), r_s the sample radius, r_c the radius of central borehole . The real thickness of the slice was calculated by:

$$l_i = l_{i,theo} \cdot k,$$

where k is an empirically determined correction factor, calculated as

$$k = \frac{\Delta l_{total}}{\sum l_{i,theo}},$$

with $\Delta l_{\mathrm{total}}$ being the measured difference in sample length before and after complete slicing and $\Sigma l_{i,\mathrm{theo}}$ being the sum of the initially calculated theoretical values $l_{i,\mathrm{theo}}$ of each slice. This was done in order to check and account for potential accumulated errors, since the results from mass determination in a number of cases showed fluctuations greater than the smallest significant value given by the scale, maybe due to the small mass differences compared to the much larger total sample mass and volume. In comparison, $\Delta l_{\mathrm{total}}$ could be determined with much greater precision, providing a good reference. The values for k obtained were 1.040 (argon atmosphere experiment) and 1.067 (air atmosphere experiment).

The slices were then extracted overnight with 1 M HNO_3 and analyzed with LSC. Finally the total Tc activity distribution in the clay sample along the diffusion direction was calculated.

3. Reactive transport model including surface complexation redox reactions

3.1. Mathematical framework

PFLOTRAN 4.0 was used to model diffusion coupled to reactions involving Tc under aerobic and anaerobic conditions. PFLOTRAN is an open source, state-of-the-art reactive transport code (Lichtner et al., 2015). The governing mass conservation equations for the geochemical transport mode for a multiphase system is written in terms of a set of independent aqueous primary or basis species with the form

$$\frac{\partial}{\partial t}\left(\varphi \sum_{\alpha} s_\alpha \psi_j^\alpha\right) + \nabla \bullet \sum_{\alpha} \Omega_j^\alpha = Q_j - \sum_m \nu_{jm} I_m - \frac{\partial S_j}{\partial t} \quad (1)$$

and

$$\frac{\partial \varphi_m}{\partial t} = V_m I_m \quad (2)$$

for minerals with molar volume V_m, reaction rate I_m and volume fraction φ_m. The term involving S_j describes sorption processes. The quantity ψ_j^α denotes the total concentration of the j^{th} primary species A_j^{pri}. Sums over α in Eq. (1) are over all phases (liquid and gas) in the system. S_α is the saturation index. Ω_j^α is the total flux for species-independent diffusion. The quantity Q_j denotes a source/sink term and φ represents the porosity. In this study, only diffusion and reactions are taken into account, and the system is fully saturated. Thus, eq. 1 could be simplified as:

$$\frac{\partial}{\partial t}\left(\varphi \psi_j\right) - \nabla \bullet \left(\varphi \tau D_j^0 \bullet \nabla \psi_j\right) = -\sum_m \nu_{jm} I_m - \frac{\partial S_j}{\partial t} \quad (3)$$

$$D_e = \varphi D_p = \varphi \tau D_j^0 \quad (4)$$

The effective diffusion coefficient D_e, the pore diffusion coefficient D_p, and the diffusion coefficient of species j in water D_j^0 are related via the porosity φ and the diffusion reduction factor τ via eq. 4.

The reaction rate I_m is based on transition state theory with form as

$$I_m = -A_m \left(\sum_l k_{ml}(T) P_{ml}\right) \left|1 - (K_m Q_m)^{\frac{1}{\sigma_m}}\right|^{\beta_m} sign(1 - K_m Q_m) \quad (5)$$

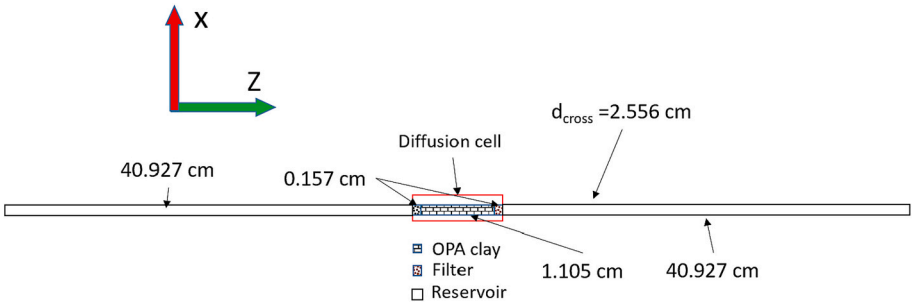

Fig. 2. Schematic view of the reactive transport model.

Table 3
Geometrical parameters of the different model components. The symbol '/' means it is a parameter and its values need further fitting and will show and discuss in result.

Parameters	air	argon
Clay porosity φ	0.16	0.20
Filter porosity φ	0.20	0.20
Reservoir porosity φ	1	1
Clay length L (cm)	1.110	1.105
Diameter d (cm)	2.545	2.556
Diffusion reduction factor in clay τ	/	/
Diffusion reduction factor in filter τ	0.247	0.247

Where summation of l means contribution from parallel mechanisms. And K_m is the equilibrium constant, σ_m is the Temkin's contant, β_m is the affinity power, A_m denotes the specific mineral surface area, and Q_m is the activity product. The rate constant k_{ml} is temperature related and given by the Arrhenius relation as eq. 6,

$$k_{ml}(T) = k^0_{ml} exp\left[\frac{E_{ml}}{R}\left(\frac{1}{T_0}-\frac{1}{T}\right)\right] \quad (6)$$

Where k^0_{ml} represents the rate constant at temperature T_0, which taken as 298.15 K, E_{ml} refers to the activation energy (J/mol), P_{ml} is the prefactor for the lth parallel reaction.

All species are modelled as diffusing species included all reaction products. All mineral reaction are formulated as kinetic reactions and all aqueous reactions are equilibrium reactions. So for the kinetic reaction of minerals, prefactor P_{ml}, activation energy E_{ml}, and the related parallel reaction species are needed. For the pyrite, only the kinetic constant is used and acts as a fit parameter in the model.

3.2. Transport part in the model

Consistent with the design of the diffusion cell, the geometry of model is a 1D cylindrical model (Fig. 2). The clay column is sandwiched between two filters. The cylinder is discretized into 140 cells in the axial direction, using 10 nodes for each filter, 100 nodes for the clay and 10 nodes for each reservoir with a length calculated by dividing the reservoir solution volume by the cross section of the diffusion cell. In the radial direction, only one node is assigned with a length calculated from the cross section of the diffusion cell.

Geometrical properties of the different components in the model are summarized in Table 3. The diffusion reduction factor τ in clay is calculated according to Eq. 4 by fitting the model with HTO diffusion results as discussed later. The diffusion reduction factor τ in filter is calculated from the D_e of HTO diffusion in filter and the filter porosity ($D_e = 1.06 \times 10^{-10}$ m^2/s, filter porosity $\varphi = 0.20$; Chen et al., 2023).

3.3. Chemical reactions in the model

The retardation of ^{99}Tc in Opalinus Clay is strongly related to the redox reactions that might occur between Fe(II) and TcO_4^- that diffuses from the solution into the rock. Fe(II) in OPA clay is present in different forms. Mazurek et al. (2023) recently showed that the majority of Fe in un-weathered OPA clay is present as Fe(II) in clay minerals, followed by Fe(II) in siderite, Fe(III) in clay minerals and nano-goethite, and Fe(II) in pyrite (as shown in Fig. S1 in supplementary material).

Fe(II) present in the porewater is therefore in equilibrium with different solid phases (pyrite, siderite and clay minerals) as schematically shown in Fig. S2 in supplementary material. The equilibrium with pyrite and siderite is defined by the solubility products (K_s) and the equilibrium with clay minerals by sorption-desorption reactions involving ion exchange and surface complexation reactions with strong (-SO) and weak (-WO) sites on the edges of clay minerals (Chen et al., 2022).

The redox reactivity of Fe(II) species depends strongly on the speciation. It is known that dissolved Fe(II) has the lowest redox reactivity whereas Fe(II) in solid phases shows the highest reactivity (Peretyazhko et al., 2008). The study of Hoving et al. (2017) on the redox properties of clay-rich sediments by mediated electrochemical analysis showed that Fe associated with clay minerals showed the highest redox reactivity. Combined with the information given in Mazurek et al. (2023), it can be assumed that the Fe(II) associated with clay minerals such as illite might be the most important reaction partner for the reduction/immobilization of TcO_4^- in OPA clay.

The clay and pore water composition in Table 1 and Table 2 are used in the chemical model. The default database for PFLOTRAN "hanford.dat" is used to define stabilities and solubilities of secondary species and minerals, respectively. Although it is thermodynamically feasible that TcO_4^- reacts with aqueous Fe^{2+} to form a Tc(IV) precipitate, this reaction was not considered in the model because it is known from the literature that sorbed Fe(II) or Fe(II) in a solid phase is more reactive (Peretyazhko et al., 2008). Therefore, a redox reaction between surface complexed Fe (II) and Tc(VII) is proposed (Eq. 7 and Eq. 8 in Table 4). The two-site protolysis non-electrostatic surface complexation and cation exchange (2SPNE SC/CE) sorption model was used (Bradbury and Baeyens, 1997). Illite was assumed to be the only mineral with active surface sites. The properties of illite were fully characterized by Baeyens and Bradbury (2004) and the related properties have been taken from Chen et al. (2022), such as cation exchange capacity (CEC), the surface hydroxyl group capacity, protolysis constants and equilibrium constant for Fe sorbed on surface. The redox reactions involved in the model are summarized in Table 4.

Dissolution reactions of the mineral components in OPA clay as shown in Table 1 are kinetically controlled. The dissolution rate constants of the minerals in OPA clay are taken from Palandri and Kharaka (2004), except for pyrite (eq. 10), whose value caused numerical problems in the simulations. As observed in Mazurek et al. (2023), goethite is the main product of Fe(III) phases after weathering. Therefore, goethite is assumed as a possible Fe(III) precipitate. The dissolution reaction of chlorite is not available in database. Instead, the data for Clinochlore-7 A was used as a proxy. The reactive surface area of 1 m^2/m^3 was assumed

Table 4
Properties of illite, redox and solubility reactions used in the reactive transport model describing the transport and Fe(II)-mediated immobilization of ^{99}Tc in OPA clay. The symbol '/' means it is a parameter and its values need further fitting and will show and discuss in result.

Site types	Site capacities
$\equiv S^SOH$	2.0×10^{-3} mol/kg
$\equiv S^{W1}OH$	4.0×10^{-2} mol/kg
$\equiv S^{W2}OH$	4.0×10^{-2} mol/kg
CEC	2.25×10^{-1} eq/kg

Protolysis reactions	Log $K_{protolysis}$
$\equiv S^SOH + H^+ \leftrightarrow \equiv S^SOH_2^+$	4.0
$\equiv S^SOH \leftrightarrow \equiv S^SO^- + H^+$	−6.2
$\equiv S^{W1}OH + H^+ \leftrightarrow \equiv S^{W1}OH_2^+$	4.0
$\equiv S^{W1}OH \leftrightarrow \equiv S^{W1}O^- + H^+$	−6.2
$\equiv S^{W2}OH + H^+ \leftrightarrow \equiv S^{W2}OH_2^+$	8.5
$\equiv S^{W2}OH \leftrightarrow \equiv S^{W2}O^- + H^+$	−10.5

Reactions	Log K	Eq.
$\equiv S^SO(TcO_2)_{0.3333}Fe^{2+} + 0.6665H_2O \leftrightarrow 0.3333TcO_4^- + 0.3333H^+ + 1Fe^{2+} + \equiv S^SOH$	/	(7)
$\equiv S^{W1}O(TcO_2)_{0.3333}Fe^{2+} + 0.6665H_2O \leftrightarrow 0.3333TcO_4^- + 0.3333H^+ + 1Fe^{2+} + \equiv S^{W1}OH$	/	(8)
$Fe^{3+} + 0.5H_2O \leftrightarrow 0.25O_2(g) + Fe^{2+} + H^+$	−7.7654	(9)
$FeS_2 + H_2O \leftrightarrow Fe^{2+} + 0.25H^+ + 0.25SO_4^{2-} + 1.75HS^-$	−24.6534	(10)
$FeCO_3 + H^+ \leftrightarrow Fe^{2+} + HCO_3^-$	−0.192	(11)
$HS^- + 2O_2(g) \leftrightarrow H^+ + SO_4^{2-}$	132.5203	(12)

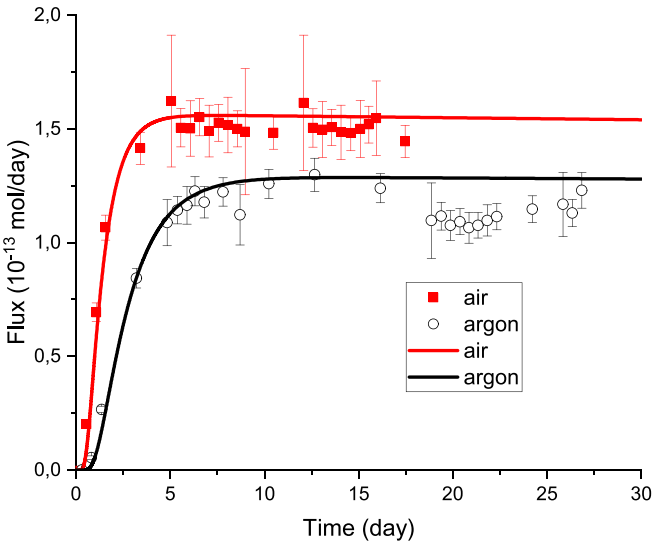

Fig. 3. Comparison of fitted and experimental flux data of HTO in OPA clay. The dot data are the experimental data, the line are the simulated data.

for all solids. The final reaction product of Tc(VII) reduced by surface complexed Fe(II) is not exactly clear. In the model it is assumed to be $\equiv S^{S}O(TcO_2)_{0.3333}Fe^{2+}$ (eq.7) and $\equiv S^{W1}O(TcO_2)_{0.3333}Fe^{2+}$ (eq. 8), even though it may also be reduced to form TcO_2, TcS_2 and/or it may be incorporated into other minerals. Note that in simulations involving aerobic conditions an artificial mineral "O_2(s)" is introduced in the source reservoir to act as a buffer for O_2(aq) at equilibrium with atmospheric O_2(g). But because of a convergence problem, the "O_2(s)" was only added to the source reservoir.

The diffusion reduction factor τ in filter and clay column was obtained by fitting the HTO diffusion data in the system described above. Then two models, model A and model B, were applied to fit the experimental data. In model A, the possible illite/smectite-alternating layer is also treated as illite. While in model B, the amount of active sites for adsorbing Fe and further reducing Tc was modified considering the oxidation condition and/or the other potential minerals, which may play the similar role as illite, such as kaolinite and chlorite. The species diffusion coefficient of $^{99}TcO_4^-$, the reaction rate of pyrite and the equilibrium constants of surface complexation redox reactions of Tc are the fitting parameters and will be manually modelled to achieve optimal agreement with the experimental results. All simulation setup and thermodynamic data were selected assuming room temperature conditions. More details will be discussed in results and discussion part.

4. Results and discussion

4.1. HTO diffusion in Opalinus clay

The comparison of fitted and measured fluxes of HTO is shown in Fig. 3. As can be seen, there is a good agreement between the model predictions and the experimental results for both air and argon atmosphere conditions.

The values of D_e for HTO diffusion in OPA clay are 3.20×10^{-11} m^2/s and 1.92×10^{-11} m^2/s for air and argon atmosphere, respectively. The D_e values are slightly larger than the value given in Van Loon et al. (2003). This good match between fitted and experimental data indicates that the model works well for diffusion of non-sorbing tracers. The porosity φ of HTO in OPA clay are 0.16 and 0.20 for air and argon atmosphere, respectively, which are consistent with values in Wu et al. (2009) and Joseph et al. (2013), whose value range from 0.15 to 0.18. The D_0 of HTO in water is about 2.15×10^{-9} m^2/s at 25 °C (Yuan-Hui and Gregory, 1974). According to Eq. 4, the diffusion reduction factor τ in filter are calculated and listed in Table 3. The diffusion reduction factor τ in clay was calculated as 0.093 and 0.045 for air and argon conditions, respectively. A higher value for the reduction factor is

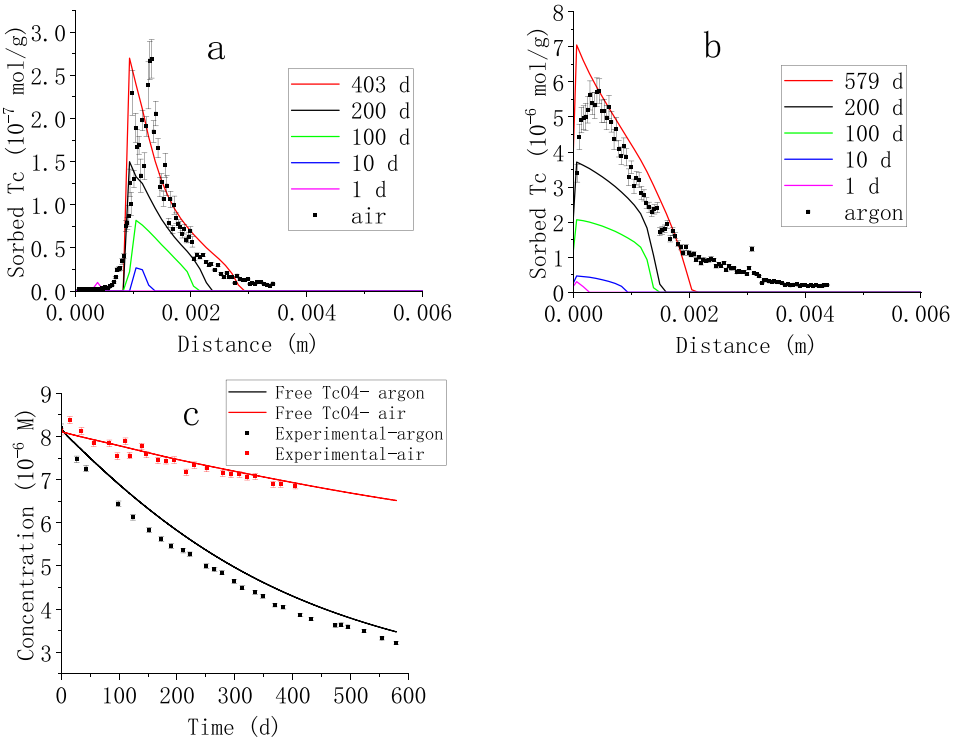

Fig. 4. Comparison of experimental data and modeling results for the model considering the reduction of Tc(VII) by surface complexed Fe(II). Simulation time corresponds to 579 and 403 days of the experiments for under argon and air atmosphere, respectively. The trend of Tc distribution for a) under air conditions; b) under argon conditions; c) concentration of TcO4- in the source reservoir.

Table 5
Parameters for best fit.

Parameter	Model A		Model B	
	air	argon	air	argon
Reaction rate pyrite ($\times 10^{-6}$ mol/m^2/s)	0.5	1.5	0.06	0.2
Species diffusion coefficient D_0(TcO_4^-) ($\times 10^{-9}$ m^2/s)	0.35	0.8	0.6	0.6
Equilibrium constant log K	−15.8	−18.6	−17.0	−17.0

expected under aerobic conditions due to the dissolution of minerals by oxygen.

4.2. Diffusion of ^{99}Tc in Opalinus clay

As shown in Fig. 4, both the final Tc distribution in OPA clay and the Tc concentration in the source reservoir as predicted with model A fit reasonably well with the experimental data for diffusion under air and under argon atmosphere. The position of the Tc peak can be reproduced quite well, but not the observed tailing. Especially for the experiments under argon atmosphere, the model tail is too sharp. The best fit parameters for this model are summarized in Table 5. Note that the obtained best fit parameters in this model are not the same for diffusion under argon and air atmosphere.

Species diffusion coefficient of aqueous O_2 is 0.11×10^{-9} m^2/s for model A and 0.10×10^{-9} m^2/s for model B. The equilibrium constant is for reactions 7 and 8 in Table 4.

It is not optimal that the model requires different transport parameters and equilibrium constants for the same species. One possible factor that might improve the model is the amount of surface sites, or the amount of active/available surface sites. As can be seen from the clay minerals reported in Table 2, besides illite there is also a substantial amount of kaolinite and chlorite, which can also sorb Fe(II) and thus can contribute to the reduction of Tc(VII). But only illite and illite/smectite mixed layer clay minerals were under consideration in model A. Thus, the amount of illite should be adjusted according to the amount of kaolinite and chlorite. The resaturation of the OPA clay with pore water for 5 weeks was conducted before the tracer diffusion experiments. While saturation of OPA clay under an argon atmosphere will prevent the oxidation of Fe(II)-species, resaturation of OPA clay under oxic atmosphere will result in partial oxidation of dissolved and sorbed Fe(II). This leads to a decrease of Fe(II)-loaded sorption sites on the clay minerals. In the model, the oxidation reaction of sorbed Fe(II) species was not implemented, only the oxidation of aqueous Fe(II) species was included. A decrease of the illite amount for under air atmosphere might somehow mimic the oxidation of sorbed Fe(II). Therefore, the amount of illite was modified in the model B. For diffusion under argon atmosphere, the amount of kaolinite was included in the amount of illite, which increases the amount of active surface sites. For diffusion under air atmosphere, the amount of illite was decreased to mimic the oxidized sorbed Fe(II). Model B gives slightly better results as shown in Fig. 5. Even though there are still significant deviations between the experimental data and the model results for both the evolution of the Tc concentration in the reservoir source reservoirs and the final Tc distribution in the OPA clay, the obtained parameters are much better and make sense: the same species diffusion coefficient for under air and argon atmosphere could be used, as well as the same equilibrium constant for reaction 7 and 8 as shown in Table 5. The different reaction rates for pyrite may be caused by the different driving forces for pyrite dissolution. For under argon condition, the driving force is TcO_4^-, while it may become O_2 for under air atmosphere.

Taking into account the different temperatures for diffusion experiments under air and argon atmosphere might also improve model B. The temperature affects the diffusion coefficient, but because the activation energy is unknown for Tc species, it was difficult to assign a value to the species diffusion coefficient at 60 °C. Temperature also affects the equilibrium constant, but no information is available that indicates whether the reactions 7 and 8 are exothermic or endothermic, neither the enthalpy values of reaction 7 and 8. Considering the temperature effects will definitely make the model more realistic and have to be included in future modeling work.

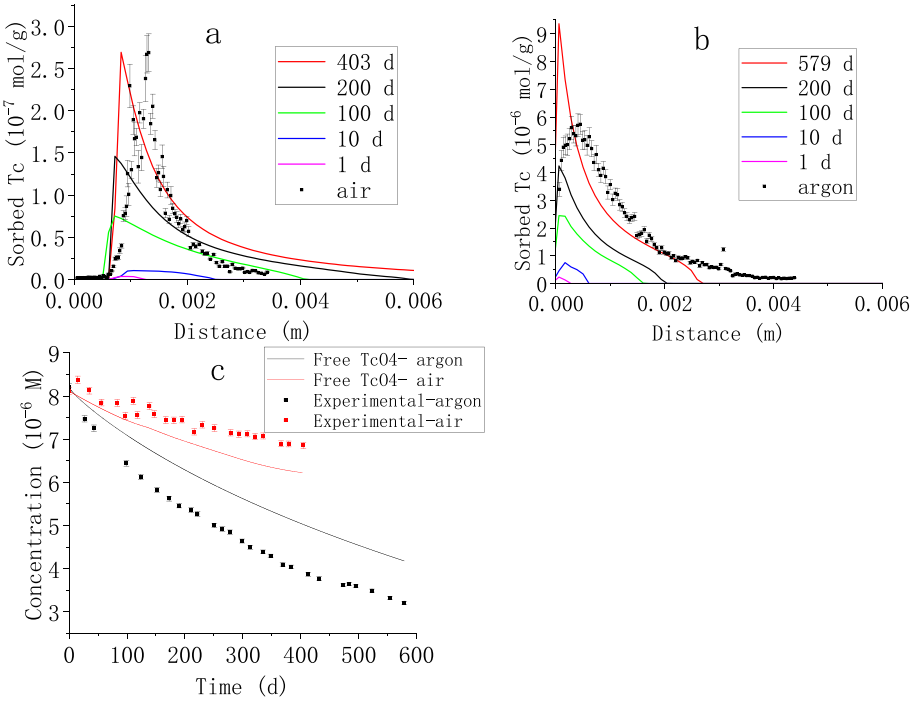

Fig. 5. Comparison of experimental data and modeling results obtained with model B (model with modified surface site capacity). Simulation runs 579 days for diffusion under argon and 403 days for under air atmosphere. The trend of Tc distribution for a) under air atmosphere; b) under argon atmosphere; c) concentration of TcO4- in high concentration reservoir.

5. Conclusions

A simple reactive transport model coupling diffusion and chemical reactions was developed in this study to reproduce experimental data of Tc diffusion through the Opalinus Clay. Some important parameters were obtained for future research, such as species diffusion coefficient of TcO_4^-, the dissolution rate of pyrite and the equilibrium constant of TcO_4^- reacting with clay surface site. Modeling results show that the final Tc distribution is a result of a complex process, in which diffusion of TcO_4^- and dissolved O_2, redox reactions, and pyrite oxidation are coupled. Under argon atmosphere, diffused TcO_4^- reacts with surface sites and sorbed Fe(II). The depletion of Fe^{2+} drives the dissolution of pyrite. This process only occurs in the clay near the source reservoir, because the diffusive flux of TcO_4^- into the core is very low and limits the rate of pyrite oxidation dissolution, whereas for diffusion experiments conducted under air atmosphere, O_2 could oxidize Fe^{2+}, which results in no Tc being retarded in the zone where O_2 is available.

Since this model is simplified, especially for the surface site capacity, more efforts could be devoted to aspects that confirm the surface site capacity or the exact clay mineral component, or confirmation of Tc speciation in clay, introducing a more representative mineralogy for the Opalinus Clay, the effect of the clay surface charge in transport and the change of porosity.

CRediT authorship contribution statement

Ping Chen: Writing – review & editing, Writing – original draft, Visualization, Software, Project administration, Investigation, Formal analysis, Data curation. **Luc R. Van Loon:** Supervision, Funding acquisition, Formal analysis, Conceptualization. **Steffen Koch:** Visualization, Methodology, Formal analysis, Data curation. **Peter Alt-Epping:** Validation, Supervision, Software, Investigation, Formal analysis, Data curation, Conceptualization. **Tobias Reich:** Supervision, Methodology, Formal analysis, Data curation, Conceptualization. **Sergey V. Churakov:** Supervision, Funding acquisition, Formal analysis.

Declaration of competing interest

The authors declare that they have no known competing financial interests or personal relationships that could have appeared to influence the work reported in this paper.

Data availability

No data was used for the research described in the article.

Acknowledgements

The Tc diffusion experiments were performed at the Johannes Gutenberg University Mainz with financial support from the German Federal Ministry of Economic Affairs and Energy (BMWi) under contract number 02E11415A. Ping Chen, the author, was financially supported by the China Scholarship Council.

Appendix A. Supplementary data

Supplementary data to this article can be found online at https://doi.org/10.1016/j.clay.2024.107327.

References

ANDRA, 2001. Référentiel géologique du site de Meuse/Haute Marne. Rapp. A RP ADS 99–005 de l'Agence nationale pour la gestion des déchets radioactifs. Châtenay-Malabry, France.

Aoki, K., 2002. Recent activities at underground research laboratories in Japan. In: Proceedings of the International Symposium NUCEF 2001. JAERI-Conf, Tokai, Ibaraki, Japan, pp. 2002–2004.

Baeyens, B., Bradbury, M.H., 2004. Cation exchange capacity measurements on illite using the sodium and cesium isotope dilution technique: effects of the index cation, electrolyte concentration and competition: modeling. Clays and Clay Minerals 52, 421–431.

Bonin, B., 1998. Deep geological disposal in argillaceous formations: studies at the Tournemire test site. J. Contam. Hydrol. 35, 315–330.

Bradbury, M.H., Baeyens, B., 1997. A mechanistic description of Ni and Zn sorption on Na-montmorillonite Part II: modelling. Journal of Contaminant Hydrology 27, 223-248. Baeyens, B., Bradbury, M.H., 2004. Cation exchange capacity measurements on illite using the sodium and cesium isotope dilution technique: effects of the index cation, electrolyte concentration and competition: modeling. Clay Clay Miner. 52, 421–431.

Bruggeman, C., Maes, N., Aertsens, M., Govaerts, J., Martens, E., Jacops, E., Van Gompel, M., Van Ravestyn, L., 2010. Technetium retention and migration behaviour in Boom Clay. In: External Report. Mol, Belgium, SCK• CEN. SCK• CEN-ER-101.

Burgeson, I.E., Deschane, J.R., Blanchard Jr., D., 2005. Removal of technetium from Hanford tank waste supernates. Sep. Sci. Technol. 40, 201–223.

Chatterjee, S., Holfeltz, V.E., Hall, G.B., Johnson, I.E., Walter, E.D., Lee, S., Reinhart, B., Lukens, W.W., Machara, N.P., Levitskaia, T.G., 2020. Identification and Quantification of Technetium Species in Hanford Waste Tank AN-102. Anal. Chem. 92, 13961–13970.

Chen, P., Van Loon, L.R., Fernandes, M.M., Churakov, S., 2022. Sorption mechanism of Fe (II) on illite: Sorption and modelling. Appl. Geochem. 143, 105389.

Chen, P., Churakov, S., Glaus, M., Van Loon, L.R., 2023. Impact of Fe(II) on 99Tc diffusion behavior in illite. Appl. Geochem. 156, 105759.

Fredrickson, J.K., Zachara, J.M., Plymale, A.E., Heald, S.M., McKinley, J.P., Kennedy, D. W., Liu, C., Nachimuthu, P., 2009. Oxidative dissolution potential of biogenic and abiogenic TcO_2 in subsurface sediments. Geochim. Cosmochim. Acta 73, 2299–2313.

Glaus, M., Aertsens, M., Appelo, C., Kupcik, T., Maes, N., Van Laer, L., Van Loon, L., 2015. Cation diffusion in the electrical double layer enhances the mass transfer rates for Sr^{2+}, Co^{2+} and Zn^{2+} in compacted illite. Geochim. Cosmochim. Acta 165, 376–388.

Grambow, B., 2016. Geological disposal of radioactive waste in clay. Elements 12, 239–245.

Hoving, A.L., Sander, M., Bruggeman, C., Behrends, T., 2017. Redox properties of clay-rich sediments as assessed by mediated electrochemical analysis: separating pyrite, siderite and structural Fe in clay minerals. Chem.Geol. 457, 149–161.

Huang, J., Jones, A., Waite, T.D., Chen, Y., Huang, X., Rosso, K.M., Kappler, A., Mansor, M., Tratnyek, P.G., Zhang, H., 2021. Fe (II) redox chemistry in the environment. Chem. Rev. 121, 8161–8233.

Joseph, C., Van Loon, L., Jakob, A., Steudtner, R., Schmeide, K., Sachs, S., Bernhard, G., 2013. Diffusion of U (VI) in Opalinus Clay: Influence of temperature and humic acid. Geochim. Cosmochim. Acta 109, 74–89.

Joseph, C., Mibus, J., Trepte, P., Müller, C., Brendler, V., Park, D.M., Jiao, Y., Kersting, A. B., Zavarin, M., 2017. Long-term diffusion of U (VI) in bentonite: Dependence on density. Sci. Total Environ. 575, 207–218.

Kasar, S., Kumar, S., Bajpai, R., Tomar, B., 2016. Diffusion of Na (I), Cs (I), Sr (II) and Eu (III) in smectite rich natural clay. J. Environ. Radioact. 151, 218–223.

Li, J., Dai, W., Xiao, G., Wang, H., Zhang, Z., Wu, T., 2012. Pertechnetate diffusion in GMZ bentonite. J. Radioan. Nucl. Ch. 293, 763–767.

Lichtner, P.C., Hammond, G.E., Lu, C., Karra, S., Bisht, G., Andre, B., Mills, R., Kumar, J., 2015. PFLOTRAN User Manual: A Massively Parallel Reactive Flow and Transport Model for Describing Surface and Subsurface Processes. Los Alamos National Lab. (LANL), Los Alamos, NM (United States); Sandia …).

Lieser, K.H., 2008. Nuclear and Radiochemistry: Fundamentals and Applications. John Wiley & Sons.

Lukens, W.W., Bucher, J.J., Shuh, D.K., Edelstein, N.M., 2005. Evolution of technetium speciation in reducing grout. Environ. Sci. Technol. 39, 8064–8070.

Mazurek, M., Wersin, P., Hadi, J., Grenèche, J.-M., Prinpreecha, N., Traber, D., 2023. Geochemistry and palaeo-hydrogeology of the weathered zone in the Opalinus Clay. Appl. Clay Sci. 232, 106793.

Morris, K., Livens, F., Charnock, J., Burke, I., McBeth, J., Begg, J., Boothman, C., Lloyd, J., 2008. An X-ray absorption study of the fate of technetium in reduced and reoxidised sediments and mineral phases. Appl. Geochem. 23, 603–617.

Nagra, 2002. Project Opalinus Clay: Safety Report: Demonstration of Disposal Feasibility for Spent Fuel, Vitrified High-Level Waste and Long-Lived Intermediate-Level Waste (Entsorgungsnachweis). Nagra Technical Report NTB 02-05, Nagra, Wettingen, Switzerland.

Ochs, M., Lothenbach, B., Wanner, H., Sato, H., Yui, M., 2001. An integrated sorption–diffusion model for the calculation of consistent distribution and diffusion coefficients in compacted bentonite. J. Contam. Hydrol. 47, 283–296.

ONDRAF/NIRAS, 2001. SAFIR-2 Second Safety Assessment and Interim Report. Belgian Agency for Radioactive Waste for Enriched Fissile Materials. Report NIROND 2001-06.

Palandri, J.L., Kharaka, Y.K., 2004. A compilation of rate parameters of water-mineral interaction kinetics for application to geochemical modeling. In: Open File Report 2004–1068. US Geological Survey.

Pearson, F., 1998. Opalinus Clay Experimental Water: A1 Type, Version 980318. PSI Internal report TM-44-98-07,. Paul Scherrer Institut, Villigen PSI, Switzerland.

Peretyazhko, T., Zachara, J.M., Heald, S.M., Jeon, B.-H., Kukkadapu, R.K., Liu, C., Moore, D., Resch, C.T., 2008. Heterogeneous reduction of Tc (VII) by Fe (II) at the solid–water interface. Geochim. Cosmochim. Acta 72, 1521–1539.

Plymale, A.E., Fredrickson, J.K., Zachara, J.M., Dohnalkova, A.C., Heald, S.M., Moore, D. A., Kennedy, D.W., Marshall, M.J., Wang, C., Resch, C.T., 2011. Competitive reduction of pertechnetate ($^{99}TcO_4^-$) by dissimilatory metal reducing bacteria and biogenic Fe (II). Environ. Sci. Technol. 45, 951–957.

Poineau, F., Rodriguez, E., Weck, P., Sattelberger, A., Forster, P., Hartmann, T., Mausolf, E., Silva, G., Jarvinen, G., Cheetham, A., 2009. Review of technetium chemistry research conducted at the University of Nevada Las Vegas. J. Radioanal. Nucl. Ch. 282, 605–609.

Shi, K., Hou, X., Roos, P., Wu, W., 2012. Determination of technetium-99 in environmental samples: a review. Anal. Chim. Acta 709, 1–20.

Tachi, Y., Yotsuji, K., 2014. Diffusion and sorption of Cs^+, Na^+, I^- and HTO in compacted sodium montmorillonite as a function of porewater salinity: Integrated sorption and diffusion model. Geochim. Cosmochim. Acta 132, 75–93.

Tachi, Y., Ochs, M., Suyama, T., 2014a. Integrated sorption and diffusion model for bentonite. Part 1: clay–water interaction and sorption modeling in dispersed systems. J. Nucl. Sci.Technol. 51, 1177–1190.

Tachi, Y., Yotsuji, K., Suyama, T., Ochs, M., 2014b. Integrated sorption and diffusion model for bentonite. Part 2: porewater chemistry, sorption and diffusion modeling in compacted systems. J. Nucl. Sci. Technol. 51, 1191–1204.

Tagami, K., 2003. Technetium-99 Behavior in the Terrestrial Environment Field Observations and Radiotracer experiments. J. Nucl. Radiochem. Sci. 4, A1–A8.

Tsai, T.-L., Tsai, S.-C., Shih, Y.-H., Chen, L.-C., Lee, C.-P., Su, T.-Y., 2017. Diffusion characteristics of HTO and $^{99}TcO_4^-$ in compacted Gaomiaozi (GMZ) bentonite. Nucl. Sci. Tech. 28, 1–8.

Van Loon, L., Eikenberg, J., 2005. A high-resolution abrasive method for determining diffusion profiles of sorbing radionuclides in dense argillaceous rocks. Appl. Radiat. Isot. 63, 11–21.

Van Loon, L.R., Soler, J.M., 2003. Diffusion of HTO, $^{36}Cl^-$, $^{125}I^-$ and $^{22}Na^+$ in Opalinus Clay: Effect of Confining Pressure, Sample Orientation, Sample Depth and Temperature. Nagra Technical Report NTB03-07, Nagra, Wettingen, Switzerland.

Van Loon, L., Soler, J., Bradbury, M., 2003. Diffusion of HTO, $^{36}Cl^-$ and $^{125}I^-$ in Opalinus Clay samples from Mont Terri: effect of confining pressure. J. Contam. Hydrol. 61, 73–83.

Wang, Z., Zhang, J., Chen, J., Zhang, Z., Zheng, Q., Li, J., Wu, T., 2017. Diffusion behavior of Re (VII) in compacted illite-, hematite-and limonite-montmorillonite mixtures. J. Radioanal. Nucl. Ch. 311, 655–661.

Wharton, M., Atkins, B., Charnockab, J., Livens, F., Pattrick, R., Collison, D., 2000. An X-ray absorption spectroscopy study of the coprecipitation of Tc and Re with mackinawite (FeS). Appl. Geochem. 15, 347–354.

Wu, T., Amayri, S., Drebert, J., Loon, L.R.V., Reich, T., 2009. Neptunium (V) sorption and diffusion in Opalinus Clay. Environ. Sci. Technol. 43, 6567–6571.

Wu, T., Wang, H., Zheng, Q., Zhao, Y.L., Li, J.Y., 2014. Effect of EDTA on the diffusion behavior of $^{99}TcO_4^-$ and ReO_4^- in GMZ bentonite. J. Radioanal. Nucl. Ch. 299, 2037–2041.

Yuan-Hui, L., Gregory, S., 1974. Diffusion of ions in sea water and in deep-sea sediments. Geochim. Cosmochim. Acta 38, 703–714.

Zachara, J.M., Heald, S.M., Jeon, B.-H., Kukkadapu, R.K., Liu, C., McKinley, J.P., Dohnalkova, A.C., Moore, D.A., 2007. Reduction of pertechnetate [Tc(VII)] by aqueous Fe(II) and the nature of solid phase redox products. Geochim. Cosmochim. Acta 71, 2137–2157.